Society of Petroleum Engineers

SPE-181551-MS

Oil Industry First Interwell Trial of Reservoir Nanoagent Tracers

Dmitry Kosynkin and Mohammed Alaskar, Saudi Aramco

This paper was prepared for presentation at the SPE Annual Technical Conference and Exhibition held in Dubai, UAE, 26-28 September 2016.

Abstract

This manuscript reports the industry's first proven reservoir nanoagents' design and describes a successful multi-well field trial using these inexpensive and environmentally friendly nanoparticles that offer an important advantage of fast and cheap fluorometric detection. Our fundamental nanoparticle tracer template, A-Dots or Arab-D dots, is intentionally geared towards the harsh but prolific Arab-D carbonate reservoir environment of 100°C temperature, 150,000 ppm salinity, and an abundant presence of divalent ions in the connate water. The A-Dots were manufactured on a scale of one metric ton from affordable and easily available commodity chemicals. They were injected into a watered-out part of the field and monitored at four nearby producer wells for two years. Monitoring of four neighbouring producer wells over a period of 26 months confirmed nanoparticles' breakthrough at a single producer nearly 500 m from the injector at the reservoir level, thus, proving the nanoparticles' mobility and transport capability. The maximum concentration of the nanoagent in produced water was observed about 10 months after the injection matching the behavior of conventional small-molecule tracers used in the same pair of wells previously. The rate of A-Dots production correlated with the rate of water injection at the original injector well and followed it closely with a 10-month delay.

This test bolstered our previous observations of satisfactory recovery of A-Dots in a single-well test by confirming their reservoir stability on industry relevant time scales and demonstrating the feasibility of their industrial production. The importance of this accomplishment is not in how sophisticated the sensing functionality of the tracer design is but rather in the nanoparticle stability, mobility, scalability, and field application potentials. Our findings render the concept of having active, reactive, and even communicative, in-situ reservoir nanoagents for underground sensing and intervention a well anticipated near-future reality.

Introduction

Nanotechnology has provided various creative solutions to the daily problems of hydrocarbon exploration and production that are being implemented in commercial products. Better understanding of physical and chemical phenomena governing the behavior of particles on 1-100 nanometer scale gave rise to superhydrophilic (Faustini et al 2015; Ji et al. 2015; Rodrigues et al. 2016) and superhydrophobic (Chen et al. 2015; Gao and Jia 2015; Gao et al. 2016; Wu et al. 2016) coatings, shale-inhibitive water-based drilling fluids (Young et al. 2013), near-wellbore fines control agens (Abad et al. 2013) and soluble metal alloys for use in hydraulic fracturing (Li and Ma 2014). In addition to imparting unique properties of

bulk materials, engineered nanoparticles hold a great promise for hydrocarbon exploration and production as individual entities acting as reservoir-traversing agents capable of changing or monitoring of reservoir conditions. A few of nanoparticle applications, such as surfactant nanoparticles, oil-sensing nanoparticles, superparamagnetic nanoparticles for electromagnetic imaging contrast enhancement and nanoparticle tracers are presently in fairly advanced stages of laboratory development. Evidently, the utility of any nanoparticle-based resorvoir agent is determined by its capacity to survive the inhospitable conditions of hydrocarbon bearing formations for the entire duration of its mission. The most challenging of them are the high salinity and hardness of connate brines, high temperature and the presence of a very expansive and chemically diverse rock surface. Even before any advanced functionality incorporation into a nanoagent can be considered, fully compatible answers to all of these challenges must be at hand. Application of suitable polymer coatings to nanoparticles that were by themselves unstable in connate brines provided them with noticeably improved stability to flocculation and adsorption. Unfortunately, the stability improvements allowed the coated particles to travel through only impractically short sand columns or small plugs of reservoir rock. A welcome breakthrogh in the development of reservoir nanoagents occurred when small fluorescent carbogenic nanoparticles (A-Dots) were discovered (Bourlinos et al. 2008). The 10-nm size of A-Dots gives them a safe passage through narrowest pores of Arab-D carbonates and their bright visible fluorescence makes their detection easy and sensitive. Even though the surface chemistry of these particles is not yet fully understood, it makes them unusually robust in the conditions of Arab-D reservoir (up to 22% TDS, up to 100°C temperature and up to 3200 psi pressure).

The origin of fluorescent emission of A-Dots and a very extensive family of similar carbogenic nanoparticles has not been satisfactorily explained despite very extensive studies published in 2004-2015 (Xu et al. 2004; Zhang et al. 2010; Zhu et al. 2011; Bourlinos et al. 2012; Jia et al. 2012; Ma et al. 2012; Markova et al. 2012; Li et al. 2013; Sachdev et al. 2013; Himaja et al. 2014; Huang et al. 2014; Hui et al. 2014; Ke et al. 2014; Liu et al. 2014; Mehta et al. 2014; Qian et al. 2014; Shi et al. 2014; Wang et al. 2014; Wei et al. 2014; Yang et al. 2014; Bao et al. 2015; Chen et al. 2015; Gong et al. 2015; Hongren et al. 2015; Jana et al. 2015; Liu et al. 2015; Shi et al. 2015; Stan et al. 2015; Yang et al. 2015; Zhang et al. 2015a; Zhang et al. 2015b; Zheng et al. 2015c). The complex and puzzling nature of these nanoparticles makes intelligent engineering of their properties very challenging. Despite being repeatedly called "carbon quantum dots", they have never been shown to have quantum confinement of excitons that would manifest itself in a predictable particle size dependency of the fluorescent emission maxima, *inter alia*. Most of these materials also have a very large content of hydrogen, oxygen and nitrogen that approaches such biopolymers as proteins, carbohydrates and humic acids. Therefore, "carbogenic nanoparticles" is a more accurate description by a wide margin. A very important advance in the understanding of the fluorescence of the A-Dots was made by us when a previously unknown highly fluorescent dye was isolated from the commercial batch of the material as a crystalline solid. Its surprising structure was unambiguously established by X-ray crystallography and it is very likely that similar conjugated heterocycles are responsible for fluorescent emission of A-Dots and related carbogenic nanoparticles (NPs).

Fluorescent carbogenic nanoparticles have been produced by either "top-down" approach where graphite (Li et al. 2011; Lin et al. 2012), heteroatom-doped graphite (Li et al. 2014), soot (Allam et al. 2013; Tripathi et al. 2014), coke (Wu et al. 2014), coal (Tour et al. 2014) and similar bulk carbon-rich materials are subjected to chemical and/or mechanical cutting and surface modification until suitably-sized nanoparticles form, or "bottom-up" approach where small-molecule or polymeric precursors are heated to generate the nanoparticles through complex bond-forming reactions. The "top-down" particles often have observable crystalline cores resembling the structure of their source material, while the "bottom-up" particles are largely amorphous. The variety of organic precursors for the latter seems to be limited only by the researchers' imagination, because it varies from citric acid (Liu et al. 2014) to simple sugars (Zhang et al. 2010), instant

coffee (Jiang et al. 2014) and even kitchen waste(Himaja et al. 2014; Ke et al. 2014) and grass clipping (Krysmann et al. 2012).

We have previously demonstrated and reported close to 86% recovery of the A-Dots from the reservoir in a huff-and-puff single well test (Kanj et al. 2011). This report provides details on a successful test of A-Dots' migration trough industrially meaningful distances of reservoir rock that confirmed their usefulness as a standalone fluorescent reservoir nanoagent.

Material Synthesis, Characterization and Scale-up

Possible Structure of A-Dots

A-Dots were discovered by Giannelis group at Cornell University as a product of thermally induced condensation of a mixture of citric acid and ethanolamine (Rashid et al. 2014). The reaction begins with simple neutralization of the acid with the amine to form a well-defined salt. The original preparation has called for mixing aqueous solutions of citric acid an ethanolamine, then followed by evaporation of water by heating in an open vessel and prolonged heating of the residual molten salt at 200-230°C. During the thermal treatment the reaction mixture turns dark brown and releases gases and steam. The chemical reactions manifested by these changes are very complex and poorly understood. Attempts at analysis of a similar reaction mixture formed by citric acid and ethylenediamine recently reported by Song *et al* (2015) resulted in isolation of an aminopyridine derivative 2 exhibiting a bright blue fluorescent emission with a maximum at 442 nm, which is very similar to A-Dots.

While the formation of compound 2 is trivial to explain by dehydration of citric acid accompanied by condensation with one molecule of ethylenediamine (Fig. 2), it does not account for the bulk of the formed products and the fluorescent emission of the product mixture at longer wavelengths and its UV-Vis spectrum.

Therefore, the development of carbogenic NPs and other fluorescent products in the reaction mixture must involve other processes that do not necessarily parallel the simple condensation outlined in Fig. 1 and do not follow the same ratio between the reactants. Peculiarly, Song *et al.* (2015) reported the highest yields of fluorescent materials when the molar ratio of ethylenediamine to citric acid was 4:1 greatly exceeding the 1:1 ratio and demonstrated a strong dependency of the yields on the pH of the reaction mixture with highest values observed at pH=8.4. A study of the effect of reaction temperature on wavelength and intensity of fluorescent emission of the products of reaction between citric acid and ethanolamine by Giannelis *et al.* (2012), suggested that temperatures below 230°C favor the formation of low-molecular weight products with high quantum yields of fluorescence, while heating at 300-400°C leads to predominance of nanoparticles with "carbon cores" exhibiting less efficient emission at longer wavelengths. It is extremely unlikely that anything resembling allotropes of pure carbon was formed even at 400°C, though, since even the pyrolysis of easily carbonizable carbohydrates or wood at 400°C has been shown to give products with high content of hydrogen and oxygen that were interpreted as sheets of polycyclic aromatic hydrocarbons (Toda et al. 2005). Thus, a more realistic model of the cores of carbogenic NPs produced during the pyrolysis of salt at 400°C should include polycyclic aromatic heterocycles possibly embedded into an amorphous polymeric matrix (Fig. 2) (Song et al. 2015). The notion of "carbon core" should be used only in the limited sense outlined above.

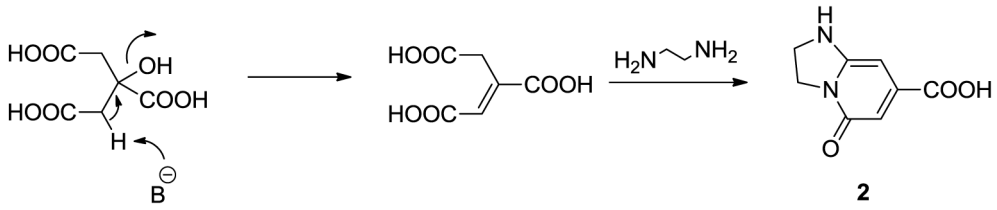

Figure 1—Formation of compound 2 from citric acid.

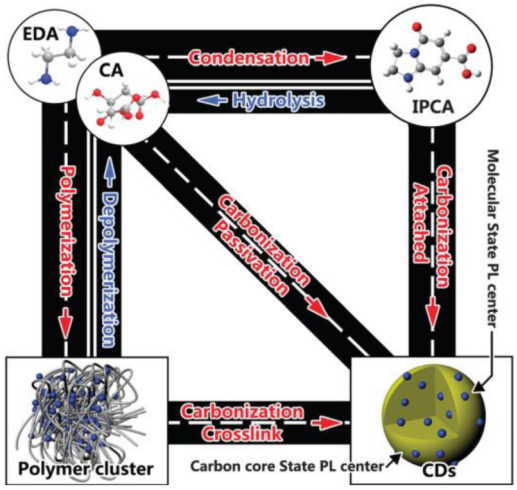

Figure 2—Relationships between products of thermal treatment of citric acid mixtures with ethylenediamine

Characterization of A-Dots

Complex product mixtures resulting from the pyrolysis of ethanolamine citrate have not yet been separated to isolate and identify the individual small-molecule precursors of A-Dots. Giannelis *et al.* (2012) subjected the product mixtures to dialysis against water through cellophane membranes with up to 10kDa cut-off. When no fluorescent or colored products could be detected in the dialysate, the retentate still had deep brown coloration and exhibited strong fluorescence with maxima dependent on the temperature of pyrolysis. Transmission Electron Microscopy (TEM) and Atomic Force Microscop (AFM) imaging revealed the presence of small (<10 nm) round particles with high carbon content. No attempt to quantify the yield of these particles has been made and all subsequent yield optimization studies relied on gross fluorescence of the whole product mixture. Song *et al.* (2015) separated the NP fraction of the products of thermal decomposition of a similar mixture of citric acid and ethylenediamine at 200°C into three distinct fractions by column chromatography and determined their elemental composition (**CAEDA NPs**, Table 1).

Table 1—Elemental compositions of carbogenic NPs, their precursors and relevant carbonaceous materials.

		Elemental Composition, %				Atomic Ratio		
	Material	**C**	**H**	**O**	**N**	**H/C**	**O/C**	**N/C**
1	Citric Acid	37.5	4.2	58.3	0	1.33	1.17	0.00
2	Ethanolamine	39.3	11.6	26.2	22.9	3.52	0.50	0.50
3	Ethylenediamine	40.0	13.4	0	46.6	4.00	0.00	1.00
4	Glucose	40.0	6.7	53.3	0	2.00	1.00	0.00
5	Aramco Orange	57.8	6.1	19.26	16.9	1.25	0.25	0.25
	CAEDA NPs							
6	**CA:EDA=4:1**	**46.0**	**5.5**	**43.4**	**5.2**	**1.42**	**0.71**	**0.10**
7	**CA:EDA=2:1**	**49.5**	**5.6**	**35.0**	**9.9**	**1.35**	**0.53**	**0.17**
8	**CA:EDA=2:1**	**40.2**	**5.7**	**43.0**	**11.1**	**1.68**	**0.80**	**0.24**
9	**CA:EDA=1:2**	**35.4**	**7.3**	**42.4**	**14.9**	**2.44**	**0.90**	**0.36**
10	**CA:EDA=1:4**	**31.8**	**7.7**	**45.3**	**15.2**	**2.90**	**1.07**	**0.41**
11	Maillard polymers	53.4	5.4	37.6	4.3	1.20	0.53	0.07
12	anthracene	94.3	5.7	0	0	0.72	0	0

(continued on next page.)

Table 1—continued.

		Elemental Composition, %				Atomic Ratio		
	Material	C	H	O	N	H/C	O/C	N/C
13	Lignite	60–75	6.0–5.8	34-17		0.93-1.20	0.21	
14	Forge coal	89.5-90.5	4.5-4.0	3.2-2.8		0.53-0.60	0.02	
15	Nonbaking coal	90.5-91.5	4.0-3.75	2.8-3.5		0.49-0.53	0.03	
16	Anthracite	>91.5	<3.75	<2.5		<0.49	<0.02	
17	Graphite	100	0	0		0	0	0

Comparison of the atomic ratios of hydrogen to carbon and oxygen to carbon between Song's carbonaceous NPs (Table 1, entries 6-10) with coals (Table 1, entries 13-16) clearly shows that the degree of carbonization in NPs is very low and is more similar to the products of advanced Maillard reaction between glucose and glycine (Table 1, entry 11) (Yaylayan and Kaminsky 1998). The NPs have more than 1.2 atoms of hydrogen per each atom of carbon, therefore the possibility of existence of extended domains comprised of pure carbon is extremely remote. Since isolation and physical counting of A-Dots in experimental samples would be completely impractical, their detection and quantification relied entirely on fluorescent spectrophotometry. Taking into consideration the latest reports appearing in the literature after the A-Dot synthesis optimization study was already completed, this approach no longer remains adequate as small-molecule fluorophores produced during heating of CA-EA mixtures emit at the same wavelengths as the A-Dots.

Fluorometric analysis of A-Dots was performed using a Quantech tabletop fluorometer equipped with a bandpass filter for the excitation beam during the yield optimization stage of the project and the single-well injection test. The later stages employed a more advanced NanoLog spectrofluorometer equipped with gratings and a more sensitive PMT detector. We found that the practical range of A-Dot reaction mixture concentration in water is from 0.1 ppb to 0.4 ppm. Lower concentrations are difficult to measure due to a very intense fluorescence of produced water in the region of the A-Dot emission maximum (Fig. 3), while the higher ones do not linearly correspond to the intensity of fluorescence.

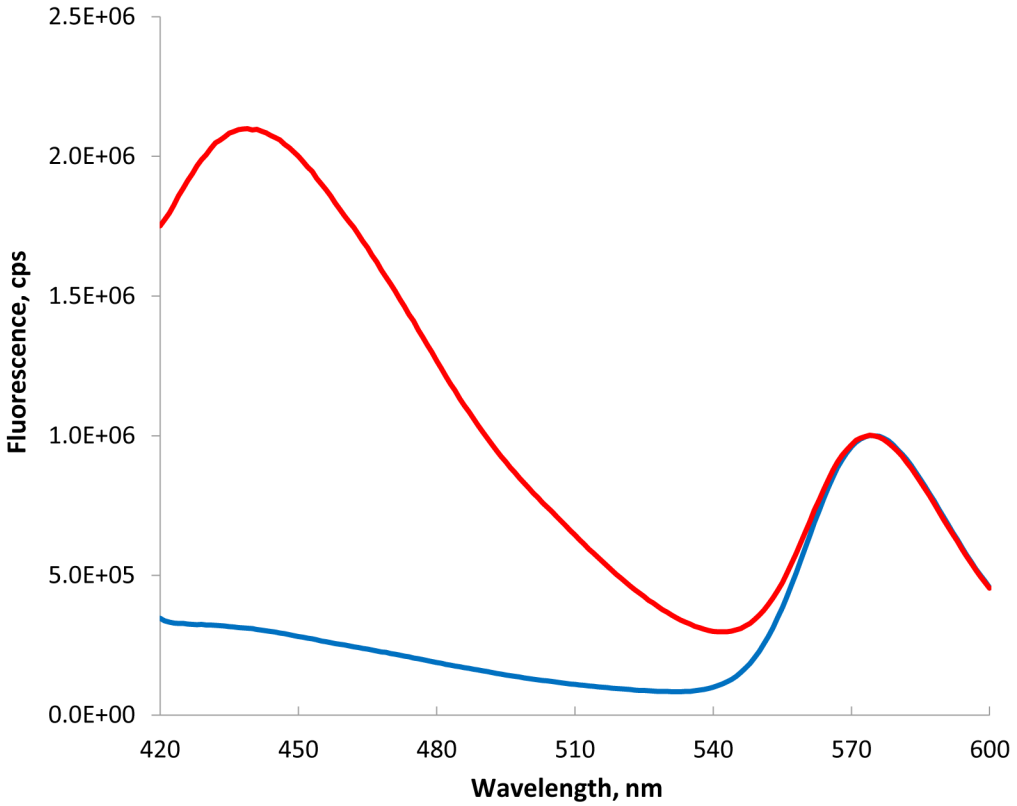

Figure 3—Fluorescent emission of A-Dots (200 ppb, orange line) and produced water control (blue line) with Rhodamine B (100 ppb) as an internal standard.

We assumed that high background fluorescence of produced water resulted from residual microscopic droplets of crude and natural water-soluble polycyclic aromatics. It was substantially reduced by fourfold extraction with dichloromethane. The fluorescence output of A-Dot is nearly linearly proportional to their concentration up to about 50 ppm (Fig. 3) making their quantification in the produced water very straightforward (Kanj et al. 2011). The quantum yield of A-Dot fluorescence is about 10% between 400 and 500 nm regardless of the excitation wavelength making this agent detectable at concentrations as low as 10 ppb. Rhodamine B (100 ppb, λ_{max}=575 nm) was added to the samples as an internal standard. All collected spectra were then normalized to have the Rhodamine B peak intensity of exactly 10^6 cps.

Z-potential measurements made with a Malvern Zetasizer (Malvern Instruments, Nanoseries) showed that the particles carry a significant negative charge at neutral pH (-26 mV) that may be caused by the presence of multiple carboxylic groups on their surface.

The product mixtures resulting from heating citric acid with ethanolamine according to the original Giannelis procedure were freed from small-molecule byproducts by repeated dialysis against DI water with 10 kDa cut-off cellophane membranes. Imaging performed with a Technai FEI T12 transmission electron microscope revealed the presence of fairly monodisperse small (5-10 nm) particles (Fig. 4a). The particles were also observed by AFM (Fig. 4b). It should be borne in mind while examining the AFM images, that only heights of surface features can be determined with reasonable accuracy. Their apparent diameters depend on the geometry of a particular AFM tip and are grossly exaggerated.

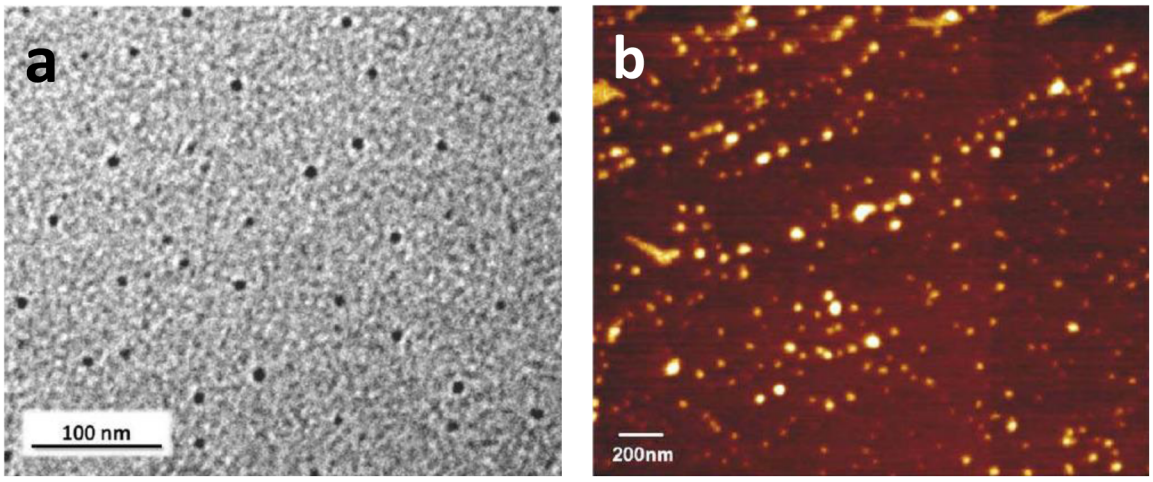

Figure 4—Microscopic images of purified A-Dots.

A-Dots Preparation Scale-up

We hypothesized that excessive positively or negatively charged functional groups exposed on the surface of the A-Dots would lead to enhanced adsorption to the surface of reservoir rock. Therefore, only 1:3 ratio of citric acid to ethanolamine resulting in the formation of a fully neutralized salt was explored. Preliminary experiments demonstrated that using citric acid as an aqueous solution according to the original synthetic procedure developed by Giannelis *et al.* (2012) was not necessary. All our optimization experiments were done by adding liquid ethanolamine to solid citric acid in disposable scintillation vials and then exposing the resulting mixture to different durations of heating at a range of temperatures.

Heating of the reaction mixture longer than 15 hours at 200°C gave noticeable amounts of insoluble tar if the reaction was run in an incompletely sealed vial, while heating for 4 hours at temperatures above 240°C produced mainly water-insoluble black tar accompanied by small amounts of dark-brown oily liquid. The brightest fluorescence at 450 nm was observed when the reaction mixture was heated at 210°C for 24 hours despite the formation of small amounts of insoluble tar mentioned above. When the reaction was repeated in the same conditions, except that the mixture was kept in a Teflon-lined steel autoclave, no insoluble materials were detected. Therefore, these reaction conditions were considered to be sufficiently optimized to begin scaling up at a pilot plant of a toll manufacturer. The upscaling studies showed that the same molar amount of anhydrous citric acid can be used instead of the specified monohydrate. It was found that diluting the final product with water to 80% concentration makes it fluid enough for packaging at 45-50°C.

Field Preparation and Testing

Interwell Field Test

Our original intent was to use an existing injector well that had an observation well in close proximity so that the interwell distance at the reservoir depth would be 150-200 meters. Considering the commonly accepted rate of fluid migration in the Arab D reservoir of 1 ft/day, this distance would allow us to complete the test in less than a year. Unfortunately, a proper disposal of produced fluids was impossible to arrange and we had to resort to using the set of wells that was employed by the CO2 EOR pilot project that was already connected to a GOSP. The wells are vertically drilled to the base of the Arab-D formation at 7500-ft depth, cased and perforated (Fig. 6). The green cylinder along each well's axis represents the perforated part of the casing. There are 4 power water injectors (I1-I4) and 4 producers (P1-P4) with each well passing about 8000 bpd of fluids on average. Treated Arabian Gulf sea water is used for the injection. The oil cut in the produced fluid is less than 5%. Prior to the injection of the A-Dots, all wells were kept in the described regime of operation for more than a year and the pairwise connectivity of the injectors and producers was

tested by chemical tracer injection. At the time of the scheduled commencement of the A-Dots test, it was found that the injector I3 was definitely connected to the producer P3. Therefore, the I3 was chosen for the A-Dots injection. All 4 producers were scheduled to be monitored for A-Dots breakthrough.

A-Dots were delivered to Aramco as a very thick syrup in 5-gallon polyethylene jugs. Pouring the syrup out proved impractical for field use because each jug would take several hours. To prepare a thinner solution, a batch of the original A-Dot concentrate (300 kg) was mixed with hot tap water using a home-made recirculating heater built from a 500-l polyethylene water tank, a 450-W water pump and a house water heater (Fig. 7). The resulting solution deposited needle-like orange crystals after several days of storage. The crystals were allowed to settle for a week and were removed by careful decantation. The decanted solution was transferred to fresh 5-gallon polyethylene jugs and delivered to the test location on a flat-bed truck. A small batch of the crystals was purified by recrystallization from a hot aqueous solution of ethanolamine (1%) to give shiny long orange needles. This material was unambigously determined to be a novel heterocyclic compound (Fig. 5) that was given a short name of Aramco Orange (AO).

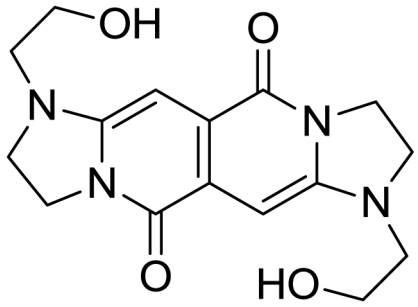

AO

Figure 5—Heterocyclic compound (Aramco Orange).

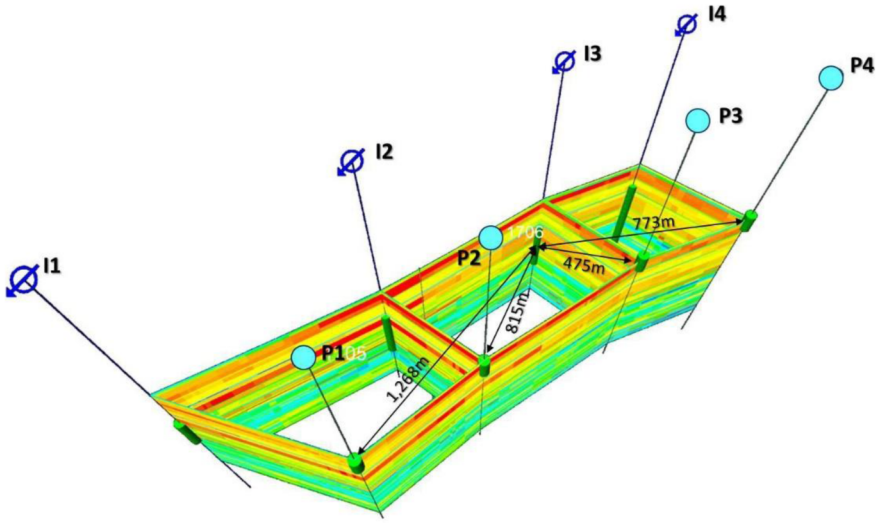

Figure 6—Interwell test configuration.

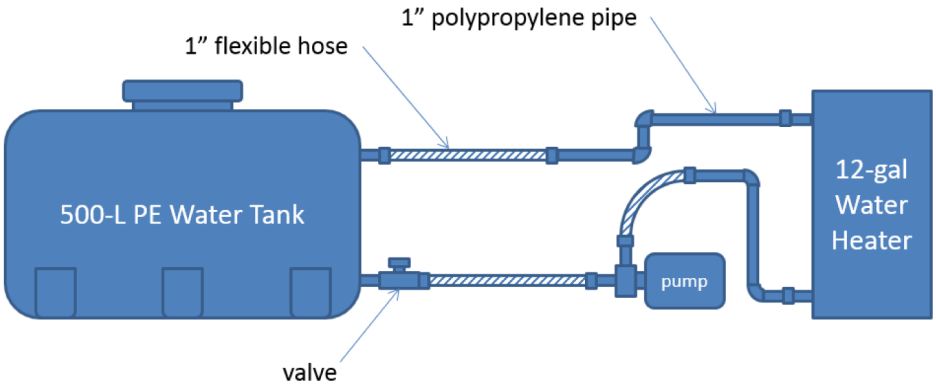

Figure 7—Recirculating device for A-Dot dissolution.

The exact mechanism of AO formation remains unknown. Solutions of AO in water, lower alcohols, DMSO and DMF show intense fluorescence with maxima located at 465 and 530 nm. The 530 nm fluorescence disappears very quickly if solutions of AO in protic solvents (alcohols, water) are exposed to 405 nm irradiation or sunlight but the 465 nm fluorescence remains unchanged. This observation combined with much higher photostability of AO solutions in aprotic solvents suggests that at least the initial step of its pholytic decomposition is photoprotonation. Results of our ongoing studies of photochemical transformations of AO and the mechanism of its formation will be reported elsewhere.

A total of 300 kg A-Dots tracer was added to 650 barrels of injection water contained in a frac tank as a prediluted solution. The A-Dots concentration in the tank was close to 3,000 ppm. The tracer solution was filtered to 50µm to avoid formation damage. The injection was done offline from the seawater injection operation at I3. The injection rate of the tracer solution into I3 averaged 6.5 barrels per minute (BPM). This rate was below the wells capacity of 10 BPM. Immediately after finishing injection, the test well was put back online and normal seawater injection resumed.

Sampling and Analysis

The detailed procedure of sample collection, treatment and analysis was described elsewhere (Kanj and Kosynkin 2015). The fluorescent signal of A-Dots significantly exceeding the background level was detected in the producer P3 at about 60 days after the nanoagent injection (Fig. 8). The intensity of A-Dots fluorescence has been increasing for almost a year thereafter confirming the breakthrough. The actual amount of A-Dots in the produced water was determined employing calibration curves built using samples of the original injection solution stored in screw-cap pressure tubes at 100°C for the entire duration of the test to account for possible alterations of fluorescent intensity caused by reactions of the nanoagent with hot water. The resulting recovery curve was compared to the recovery curves of conventional chemical tracers A and B (Fig. 8). Whereas the overall shape of the curves and the position of their maxima were similar, the A-Dots recovery showed two pronounced dips at 525 and 777 days after the nanoagent injection and it also had persistent fluctuations of considerable magnitude not seen with the chemical tracers. A possible explanation for the dips was found in the water injection log of I3 as the injection has been stopped for several weeks on two separate occasions (Fig. 9).

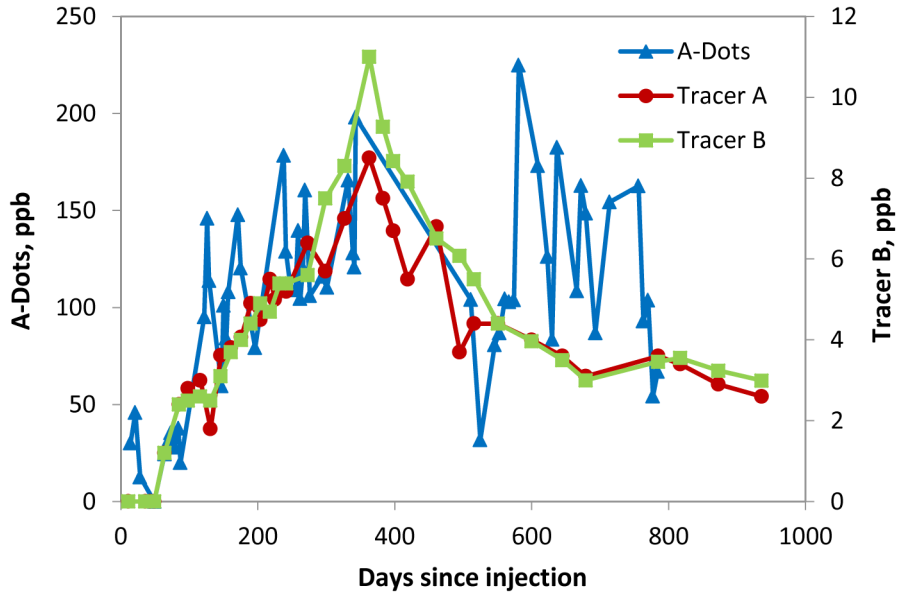

Figure 8—Recovery curves of A-Dots (blue line), tracer A (maroon line) and tracer B (green line).

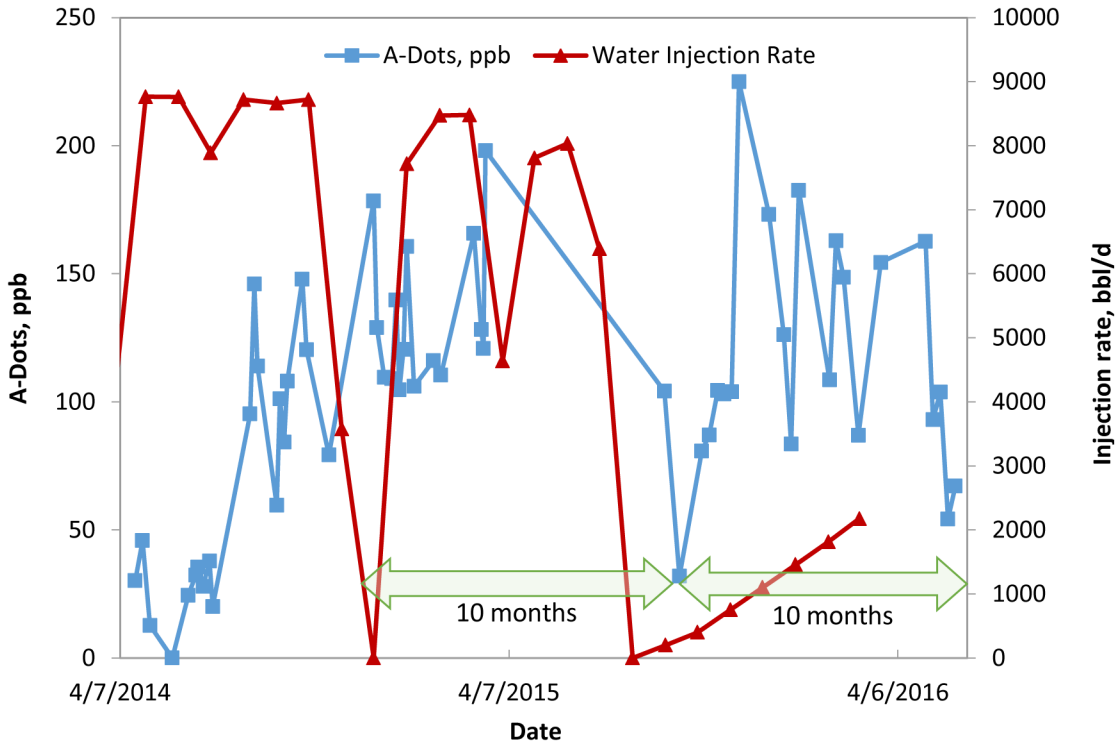

Figure 9—Recovery curve of A-Dots (blue line) vs. water injection rate at I3 (maroon line). Length of green arrows equals 10 months.

It is obvious that after the initial period of slow recovery common for all studied tracers, the A-Dots begin arriving at a significantly higher relative rate than tracers A and B. The reason for this discrepancy may lie in the much larger size of A-Dot particles in comparison with small molecules of the chemical tracers that makes them less prone to diffuse into submicron formation pores, thus avoiding retardation.

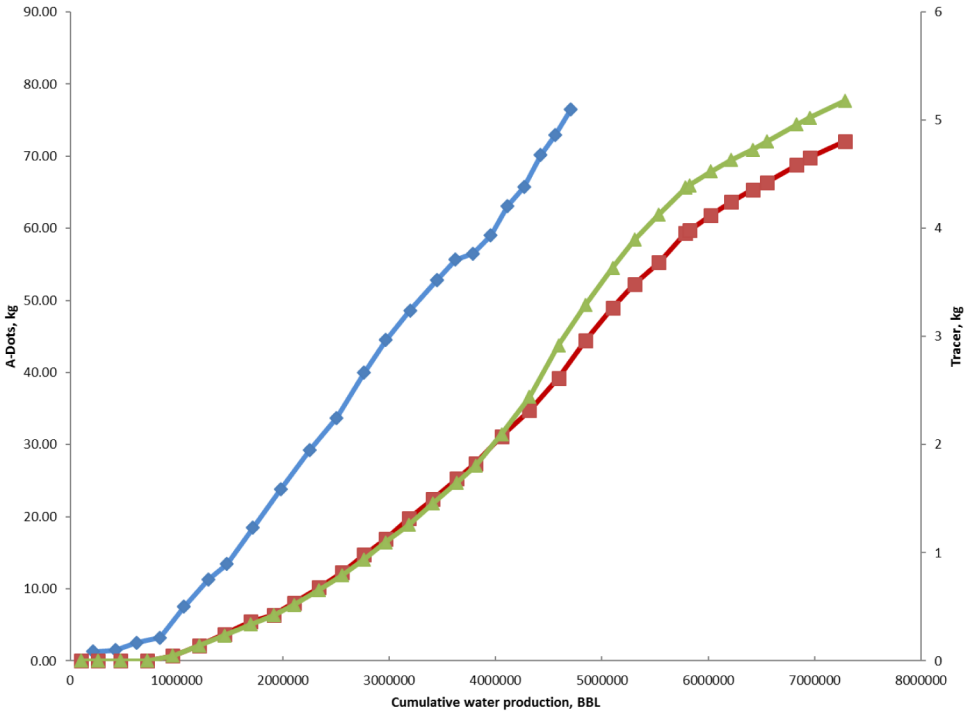

Figure 10—Cumulative recovery of A-Dots (blue line), tracer A (maroon line) and tracer B (green line).

Conclusions

Our test proved long-term stability of A-Dots in Arab-D reservoir conditions, demonstrated feasibility of large-scale industrial production of the nanoagent and compared the reservoir transport properties of A-Dots with small-molecule chemical tracers thus achieving all initially set goals. Additionally, we observed a strong indication of decreased retardation of A-Dots that was expected from Einstein-Smoluchowski theory but never seen in actual petroleum reservoir conditions.

Acknowledgments

The authors acknowledge the valuable support that the project received from Saudi Aramco's Southern Area Production Engineering, Ibrahim Zefzafy and Abdullah Alghamid, South Ghawar Producing, Hussain Lowaimi, and Southern Area Reservoir Management Departments. This support not only made the field trial possible but it also brought it to a successful completion. The authors are also particularly grateful to the following individuals: Mr. Fouad A. Sadis (lab support), Mr. Mustafa Alsaffar (lab support) and Dr. Mazen Kanj (planning during the injection phase of the project).

References

1. Chen, Z.; Liu, X. J.; Wang, Y.; Li, J.; Guan, Z. S., Highly transparent, stable, and superhydrophobic coatings based on gradient structure design and fast regeneration from physical damage. *Applied Surface Science* 2015, **359**, 826-833.
2. Gao, D. H.; Jia, M. Q., Preparation of hierarchical porous Zn-salt particles and their superhydrophobic performance. *Applied Surface Science* 2015, **359**, 89–97.
3. Gao, L. K.; Gan, W. T.; Xiao, S. L.; Zhan, X. X.; Li, J., A robust superhydrophobic antibacterial Ag-TiO2 composite film immobilized on wood substrate for photodegradation of phenol under visible-light illumination. *Ceramics International* 2016, **42** (2), 2170–2179.

4. Wu, X. H.; Fu, Q. T.; Kumar, D.; Ho, J. W. C.; Kanhere, P.; Zhou, H. F.; Chen, Z., Mechanically robust superhydrophobic and superoleophobic coatings derived by sol-gel method. *Materials & Design* 2016, **89**, 1302–1309.
5. Faustini, M.; Grenier, A.; Naudin, G.; Li, R. H.; Grosso, D., Ultraporous nanocrystalline TiO2-based films: synthesis, patterning and application as anti-reflective, self-cleaning, superhydrophilic coatings. *Nanoscale* 2015, **7** (46), 19419–19425.
6. Ji, W. H.; Zhang, M. M.; Wang, D. J.; Wang, X.; Liu, J. H.; Huang, L. Q., Superhydrophilic molecularly imprinted polymers based on a water-soluble functional monomer for the recognition of gastrodin in water media. *Journal of Chromatography A* 2015, **1425**, 88–96.
7. Rodrigues, B. V. M.; Silva, A. S.; Melo, G. F. S.; Vasconscellos, L. M. R.; Marciano, F. R.; Lobo, A. O., Influence of low contents of superhydrophilic MWCNT on the properties and cell viability of electrospun poly (butylene adipate-co-terephthalate) fibers. *Materials Science & Engineering C-Materials for Biological Applications* 2016, **59**, 782–791.
8. Li, G.; Ma, Z.; Sun, S. Soluble magnesium base alloy material for preparation of fracturing ball comprises magnesium, aluminum, zinc, manganese, and cobalt. CN103898384-A.
9. Abad, C.; Ali, S.; Busby, B.; Christanti, Y.; Gadiyar, B. Fines migration controlling method for earth formation, involves treating earth formation intersecting wellbore with treatment fluid, and leaking off portion of treatment fluid into earth formation. US2010163233-A1; US8579029-B2.
10. Young, S.; Friedheim, J.; Patel, A. D.; Tour, J.; Kosynkin, D.; Patel, A. Stabilizing shales while drilling wellbore into earthen formation, comprises circulating wellbore fluid into wellbore while drilling through shales, where wellbore fluid comprises graphene-based material. WO2012048068-A2; WO2012048068-A3; CA2813944-A1; EP2625242-A2; US2013264121-A1; MX2013003841-A1; CN103298905-A.
11. Bourlinos, A. B.; Stassinopoulos, A.; Anglos, D.; Zboril, R.; Karakassides, M.; Giannelis, E. P., Surface functionalized carbogenic quantum dots. *Small* 2008, **4** (4), 455–458.
12. Xu, X.; Ray, R.; Gu, Y.; Ploehn, H. J.; Gearheart, L.; Raker, K.; Scrivens, W. A., Electrophoretic Analysis and Purification of Fluorescent Single-Walled Carbon Nanotube Fragments. *Journal of the American Chemical Society* 2004, **126** (40), 12736–12737.
13. Zhang, J.; Shen, W.; Pan, D.; Zhang, Z.; Fang, Y.; Wu, M., Controlled synthesis of green and blue luminescent carbon nanoparticles with high yields by the carbonization of sucrose. *New Journal of Chemistry* 2010, **34** (4), 591–593.
14. Zhu, S.; Zhang, J.; Qiao, C.; Tang, S.; Li, Y.; Yuan, W.; Li, B.; Tian, L.; Liu, F.; Hu, R.; Gao, H.; Wei, H.; Zhang, H.; Sun, H.; Yang, B., Strongly green-photoluminescent graphene quantum dots for bioimaging applications. *Chemical Communications* 2011, **47** (24), 6858–6860.
15. Bourlinos, A. B.; Bakandritsos, A.; Kouloumpis, A.; Gournis, D.; Krysmann, M.; Giannelis, E. P.; Polakova, K.; Safarova, K.; Hola, K.; Zboril, R., Gd(iii)-doped carbon dots as a dual fluorescent-MRI probe. *Journal of Materials Chemistry* 2012, **22** (44), 23327–23330.
16. Jia, X.; Li, J.; Wang, E., One-pot green synthesis of optically pH-sensitive carbon dots with upconversion luminescence. *Nanoscale* 2012, **4** (18), 5572–5575.
17. Ma, Z.; Ming, H.; Huang, H.; Liu, Y.; Kang, Z., One-step ultrasonic synthesis of fluorescent N-doped carbon dots from glucose and their visible-light sensitive photocatalytic ability. *New Journal of Chemistry* 2012, **36** (4), 861–864.
18. Markova, Z.; Bourlinos, A. B.; Safarova, K.; Polakova, K.; Tucek, J.; Medrik, I.; Siskova, K.; Petr, J.; Krysmann, M.; Giannelis, E. P.; Zboril, R., Synthesis and properties of core-shell fluorescent hybrids with distinct morphologies based on carbon dots. *Journal of Materials Chemistry* 2012, **22** (32), 16219–16223.

19. Li, W.; Yue, Z.; Wang, C.; Zhang, W.; Liu, G., An absolutely green approach to fabricate carbon nanodots from soya bean grounds. *RSC Advances* 2013, **3** (43), 20662–20665.
20. Sachdev, A.; Matai, I.; Kumar, S. U.; Bhushan, B.; Dubey, P.; Gopinath, P., A novel one-step synthesis of PEG passivated multicolour fluorescent carbon dots for potential biolabeling application. *RSC Advances* 2013, **3** (38), 16958–16961.
21. Himaja, A. L.; Karthik, P. S.; Sreedhar, B.; Singh, S., Synthesis of Carbon Dots from Kitchen Waste: Conversion of Waste to Value Added Product. *J Fluoresc* 2014, **24** (6), 1767–1773.
22. Huang, H.; Xu, Y.; Tang, C.-J.; Chen, J.-R.; Wang, A.-J.; Feng, J.-J., Facile and green synthesis of photoluminescent carbon nanoparticles for cellular imaging. *New Journal of Chemistry* 2014, **38** (2), 784–789.
23. Hui, D.; Peng, Z.; Tian-Yi, W.; Ji-Lie, K.; Huan-Ming, X., Nitrogen-doped carbon dots derived from polyvinyl pyrrolidone and their multicolor cell imaging. *Nanotechnology* 2014, **25** (20), 205604.
24. (a) Ke, Y.; Garg, B.; Ling, Y.-C., Waste chicken eggshell as low-cost precursor for efficient synthesis of nitrogen-doped fluorescent carbon nanodots and their multi-functional applications. *RSC Advances* 2014, **4** (102), 58329-58336; (b) Liu, J.; Liu, X.; Luo, H.; Gao, Y., One-step preparation of nitrogen-doped and surface-passivated carbon quantum dots with high quantum yield and excellent optical properties. *RSC Advances* 2014, 4 (15), 7648–7654.
25. Liu, N.; Liu, J.; Kong, W.; Li, H.; Huang, H.; Liu, Y.; Kang, Z., One-step catalase controllable degradation of C3N4 for N-doped carbon dot green fabrication and their bioimaging applications. *Journal of Materials Chemistry B* 2014, **2** (35), 5768–5774.
26. Mehta, V. N.; Jha, S.; Singhal, R. K.; Kailasa, S. K., Preparation of multicolor emitting carbon dots for HeLa cell imaging. *New Journal of Chemistry* 2014, **38** (12), 6152–6160.
27. Qian, Z.; Ma, J.; Shan, X.; Feng, H.; Shao, L.; Chen, J., Highly Luminescent N-Doped Carbon Quantum Dots as an Effective Multifunctional Fluorescence Sensing Platform. *Chemistry – A European Journal* 2014, **20** (8), 2254–2263.
28. Shi, Q.-Q.; Li, Y.-H.; Xu, Y.; Wang, Y.; Yin, X.-B.; He, X.-W.; Zhang, Y.-K., High-yield and high-solubility nitrogen-doped carbon dots: formation, fluorescence mechanism and imaging application. *RSC Advances* 2014, **4** (4), 1563–1566.
29. Wang, W.; Li, Y.; Cheng, L.; Cao, Z.; Liu, W., Water-soluble and phosphorus-containing carbon dots with strong green fluorescence for cell labeling. *Journal of Materials Chemistry B* 2014, **2** (1), 46–48.
30. Wei, J.; Zhang, X.; Sheng, Y.; Shen, J.; Huang, P.; Guo, S.; Pan, J.; Liu, B.; Feng, B., Simple one-step synthesis of water-soluble fluorescent carbon dots from waste paper. *New Journal of Chemistry* 2014, **38** (3), 906–909.
31. Yang, Z.; Xu, M.; Liu, Y.; He, F.; Gao, F.; Su, Y.; Wei, H.; Zhang, Y., Nitrogen-doped, carbon-rich, highly photoluminescent carbon dots from ammonium citrate. *Nanoscale* 2014, **6** (3), 1890–1895.
32. Bao, L.; Liu, C.; Zhang, Z.-L.; Pang, D.-W., Photoluminescence-Tunable Carbon Nanodots: Surface-State Energy-Gap Tuning. *Advanced Materials* 2015, **27** (10), 1663–1667.
33. Chen, Z.; Wang, X.; Li, H.; Li, C.; Lu, Q.; Yang, G.; Long, J.; Meng, L., Controllable and mass fabrication of highly luminescent N-doped carbon dots for bioimaging applications. *RSC Advances* 2015, **5** (29), 22343–22349.
34. Gong, X.; Lu, W.; Liu, Y.; Li, Z.; Shuang, S.; Dong, C.; Choi, M. M. F., Low temperature synthesis of phosphorous and nitrogen co-doped yellow fluorescent carbon dots for sensing and bioimaging. *Journal of Materials Chemistry B* 2015, **3** (33), 6813–6819.

35. Hongren, L.; Feng, L.; Aimin, D., A solvothermal method to synthesize fluorescent carbon nanoparticles and application to photocatalysis and electrocatalysis. *Luminescence* 2015, **30** (6), 740–744.
36. Jana, J.; Ganguly, M.; Pal, T., Intriguing cysteine induced improvement of the emissive property of carbon dots with sensing applications. *Physical Chemistry Chemical Physics* 2015, **17** (4), 2394–2403.
37. Liu, Y.; Liu, Y.; Park, S.-J.; Zhang, Y.; Kim, T.; Chae, S.; Park, M.; Kim, H.-Y., One-step synthesis of robust nitrogen-doped carbon dots: acid-evoked fluorescence enhancement and their application in Fe3+ detection. *Journal of Materials Chemistry A* 2015, **3** (34), 17747–17754.
38. Shi, Y.; Li, C.; Liu, S.; Liu, Z.; Zhu, J.; Yang, J.; Hu, X., Facile synthesis of fluorescent carbon dots for determination of curcumin based on fluorescence resonance energy transfer. *RSC Advances* 2015, **5** (79), 64790–64796.
39. Stan, C. S.; Albu, C.; Coroaba, A.; Popa, M.; Sutiman, D., One step synthesis of fluorescent carbon dots through pyrolysis of N-hydroxysuccinimide. *Journal of Materials Chemistry C* 2015, **3** (4), 789–795.
40. Yang, C.; Thomsen, R. P.; Ogaki, R.; Kjems, J.; Teo, B. M., Ultrastable green fluorescence carbon dots with a high quantum yield for bioimaging and use as theranostic carriers. *Journal of Materials Chemistry B* 2015, **3** (22), 4577–4584.
41. Zhang, B.-X.; Zhang, G.-Y.; Gao, H.; Wu, S.-H.; Chen, J.-H.; Li, X.-L., One-step hydrothermal synthesis and optical properties of PEG-passivated nitrogen-doped carbon dots. *RSC Advances* 2015a, **5** (10), 7395–7400.
42. Zhang, C.; Hu, Z.; Song, L.; Cui, Y.; Liu, X., Valine-derived carbon dots with colour-tunable fluorescence for the detection of Hg2+ with high sensitivity and selectivity. *New Journal of Chemistry* 2015b, **39** (8), 6201–6206.
43. Zheng, B.; Liu, T.; Paau, M. C.; Wang, M.; Liu, Y.; Liu, L.; Wu, C.; Du, J.; Xiao, D.; Choi, M. M. F., One pot selective synthesis of water and organic soluble carbon dots with green fluorescence emission. *RSC Advances* 2015c, **5** (15), 11667–11675.
44. Li, H.; Liu, Y.; Kang, Z.; He, X. Preparation of carbon quantum dot for making photocatalyst by mixing absolute ethyl alcohol and distilled water, connecting power cords to graphite carbon rods, performing electrochemical reaction, and separating by column chromatography. CN102127431-A.
45. Lin, L. X.; Zhang, S. W., Creating high yield water soluble luminescent graphene quantum dots via exfoliating and disintegrating carbon nanotubes and graphite flakes. *Chemical Communications* 2012, **48** (82), 10177–10179.
46. Li, M.; Yu, C.; Hu, C.; Qiu, J.; Wang, X. Nitrogen-doped fluorescent carbon dot for use in e.g. photoelectric device, detecting/sense application and oxidation-reduction catalyst, comprises pyridine nitrogen and graphite carbon, and has average particle size in preset range. CN104028291-A.
47. Allam, A.; Sarkar, S.; Sabyasachi, S. Water-soluble self fluorescing quantum carbon dot useful for tagging molecule or biological system, comprises carbon dot isolated from carbon soot treated with hydrophilic carboxylic acid groups on its surface. US2011217721-A1; US8357507-B2; IN201100618-I1.
48. Tripathi, K. M.; Sonker, A. K.; Sonkar, S. K.; Sarkar, S., Pollutant soot of diesel engine exhaust transformed to carbon dots for multicoloured imaging of E-coli and sensing cholesterol. *Rsc Advances* 2014, **4** (57), 30100–30107.

49. Wu, M. B.; Wang, Y.; Wu, W. T.; Hu, C.; Wang, X. N.; Zheng, J. T.; Li, Z. T.; Jiang, B.; Qiu, J. S., Preparation of functionalized water-soluble photoluminescent carbon quantum dots from petroleum coke. *Carbon* 2014, **78**, 480–489.
50. Tour, J. M.; Ye, R.; Xiang, C.; Lin, J.; Peng, Z. Manufacture of graphene quantum dots used for road stickers, road signs, coatings, clothing, paints and photographic processing materials, involves exposing carbon source chosen from coal and coke to oxidant. WO2014179708-A1.
51. Jiang, C. K.; Wu, H.; Song, X. J.; Ma, X. J.; Wang, J. H.; Tan, M. Q., Presence of photoluminescent carbon dots in Nescafe (R) original instant coffee: Applications to bioimaging. *Talanta* 2014, **127**, 68–74.
52. Krysmann, M. J.; Kelarakis, A.; Giannelis, E. P., Photoluminescent carbogenic nanoparticles directly derived from crude biomass. *Green Chemistry* 2012, **14** (11), 3141–3145.
53. Kanj, M. Y., Rashid, M. H., & Giannelis, E. (2011). Industry First Field Trial of Reservoir Nanoagents. Society of Petroleum Engineers. doi: 10.2118/142592-MS
54. Rashid, H.; Kanj, M. Y.; Rashid, M. H.; Giannelis, E.; Kanj, M.; Giannelis, E. P.; Janneles, E. P. Fluorescent nanoagent for use in a subsurface petroleum reservoir, comprises a carbon-based nanoparticle core, where nanoparticle core includes functional groups appended to the surface. WO2012158478-A1; US2012318503-A1; EP2707453-A1; CN103958643-A; US2015232747-A1; US2015232748-A1; US2015232750-A1; US2015233240-A1; US2015239826-A1.
55. Song, Y. B.; Zhu, S. J.; Zhang, S. T.; Fu, Y.; Wang, L.; Zhao, X. H.; Yang, B., Investigation from chemical structure to photoluminescent mechanism: a type of carbon dots from the pyrolysis of citric acid and an amine. *Journal of Materials Chemistry C* 2015, **3** (23), 5976–5984.
56. Krysmann, M. J.; Kelarakis, A.; Dallas, P.; Giannelis, E. P., Formation Mechanism of Carbogenic Nanoparticles with Dual Photoluminescence Emission. *Journal of the American Chemical Society* 2012, **134** (2), 747–750.
57. Toda, M.; Takagaki, A.; Okamura, M.; Kondo, J. N.; Hayashi, S.; Domen, K.; Hara, M., Green chemistry: Biodiesel made with sugar catalyst. *Nature* 2005, **438** (7065), 178–178.
58. Yaylayan, V. A.; Kaminsky, E., Isolation and structural analysis of Maillard polymers: caramel and melanoidin formation in glycine/glucose model system. *Food Chemistry* 1998, **63** (1), 25–31.